Available online at www.sciencedirect.com
ScienceDirect
Journal of Solid State Chemistry 181 (2008) 122–129
JOURNAL OF SOLID STATE CHEMISTRY
www.elsevier.com/locate/jssc

Synthesis and gas sensitivities of SnO_2 nanorods and hollow microspheres

Haizhen Wang, Jianbo Liang, Hai Fan, Baojuan Xi, Maofeng Zhang, Shenglin Xiong, Yongchun Zhu, Yitai Qian*

Hefei National Laboratory for Physical Sciences at Microscale, Department of Chemistry, University of Science and Technology of China, Hefei, Anhui 230026, PR China

Received 23 July 2007; received in revised form 19 October 2007; accepted 12 November 2007
Available online 17 November 2007

Abstract

SnO_2 urchin-like structures composed of nanorods with diameters of 10–15 nm and lengths of 50–70 nm have been hydrothermally synthesized via a H_2O_2-assisted route without any surfactant, using $SnCl_2$ as raw material. With the addition of methenamine (HMT), SnO_2 hollow microspheres with diameters of 2–3 μm and shell thickness of 60–140 nm were also prepared. The as-obtained products were examined using diverse techniques including X-ray powder diffraction (XRD), Raman spectroscopy, field-emission scanning electron microscopy (FE-SEM), transmission electron microscopy (TEM), selected-area electron diffraction (SAED), high-resolution TEM and photoluminescence spectra. The gas sensitivity experiments have demonstrated that the as-synthesized SnO_2 materials exhibit good sensitivity to alcohol vapors, which may offer potential applications in gas sensors.

Keywords: SnO_2; Nanorods; Hollow microspheres; Photoluminescence; Gas sensitivity

1. Introduction

In recent years, semiconductor nanomaterials have attracted much attention because of their potential scientific significance and technological applications. Tin dioxide, an important wide bandgap semiconductor with high chemical stability and excellent optical and electrical properties, has been widely applied for various devices, such as gas sensors [1,2], transparent conducting electrodes [3,4] and dye-sensitized solar cells [5,6]. As the optical, gas sensing and other properties of SnO_2 materials are strongly dependent on their size and shape, it is obvious that the controlled synthesis of the nano/microstructure of SnO_2 materials is very important for special applications.

Over the past few years, remarkable progress has been made in the synthesis of SnO_2 materials. Up to now, a variety of methods have been used to prepare SnO_2 materials with different morphologies [7–19]. For example, SnO_2 nanoribbons have been prepared via rapid oxidation of elemental tin [10]. SnO_2 nanotubes have been fabricated by an infiltration technique [12]. Beak-like SnO_2 nanorods were synthesized by a vapor–liquid–solid approach [14]. Hollow SnO_2 microspheres have been synthesized by the heat treatment of a mixture composed of tin tetrachloride pentahydrate and resorcinol–formaldehyde gel [15]. SnO_2 nanowires have been obtained by employing a molecular precursor, $[Sn(OtBu)_4]$, in a CVD process [19]. Generally, the preparation methods mentioned above involve high temperature, complicated procedures, sophisticated equipment and rigorous experimental conditions. Thus, the development of mild synthetic routes to SnO_2 materials was of great significance.

Recently, solution-based chemical routes for the synthesis of SnO_2 nanomaterials have been developed and various SnO_2 materials [20–30] have been prepared in previous research. For instance, hierarchical SnO_2 flower-like architectures have been prepared through a hydrothermal method [20]. SnO_2 dendritic nanostructures have been synthesized by controlling release rate of hydroxide

*Corresponding author. Fax: +86 551 360 7402.
E-mail address: ytqian@ustc.edu.cn (Y. Qian).

0022-4596/$ - see front matter © 2007 Elsevier Inc. All rights reserved.
doi:10.1016/j.jssc.2007.11.010

ions in ethanol solution [21]. Polycrystalline SnO_2 nanowires have been developed via a solution-phase precursor route [22]. SnO_2 nanorods have been fabricated through a microemulsion-mediated solvothermal process [23]. SnO_2 nanorods with dimensions approaching those of molecules have been prepared in water–alcohol mixtures [24]. SnO_2 nanorod arrays have been synthesized via a controlled aqueous growth process [25]. Hollow SnO_2 spheres have been fabricated by hydrothermal methods [26–29]. SnO_2 nanospheres have also been prepared via a room-temperature wet-chemical route [30]. Starting from $SnCl_2$ and H_2O_2 in the presence of CTAB, Ye et al. have fabricated SnO_2 nanobelts [31].

Herein, SnO_2 nanocrystals have been selectively synthesized via a H_2O_2-assisted hydrothermal method in the absence of any surfactant. Starting from $SnCl_2$ and H_2O_2, uniform SnO_2 nanorods with diameters of 10–15 nm and lengths of 50–70 nm could be obtained. When $(CH_2)_6N_4$ (HMT) was added in the reaction solution, SnO_2 hollow microspheres with diameters in the range of 2–3 μm could also be prepared. We found that the as-prepared SnO_2 materials exhibit excellent sensitivity to alcohol vapors and thus are expected to be useful in industrial applications such as gas sensors.

2. Experiment section

2.1. Preparation of nanorods (labeled as sample 1)

All the reagents were purchased from Shanghai Chemistry Co. with analytical-grade purity and were used without further purification. In a typical preparation procedure, 6 mmol $SnCl_2$ was dissolved into 40 mL distilled water under continuous magnetic stirring to form white slurry, which was then transferred to 50 mL Teflon-lined stainless steel autoclave. Subsequently, 5 mL of 30% H_2O_2 and 36 mmol NaOH were added, which were stirred until NaOH dissolved. The autoclave was sealed and maintained at 200 °C for 30 h and afterwards allowed to be cooled to room temperature naturally. There was white precipitation at the bottom of the autoclave and then centrifugated at a rotation rate of 4000 rpm, washed several times with distilled water and absolute ethanol, and finally dried in a vacuum desiccator at 80 °C for 12 h.

2.2. Preparation of hollow microspheres (labeled as sample 2)

The procedure was similar to the above procedure except that 7 mmol $(CH_2)_6N_4$ was added to the reaction solution and finally we would obtain hollow microspheres.

2.3. Characterization

Powder X-ray diffraction (XRD) measurements were carried out with a Philips X'Pert diffractmeter (Cu$K\alpha$ $\lambda = 1.541874$ Å; Nickel filter; 40 kV, 40 mA). The scanning electron microscope (SEM) images of the products were recorded on a Hitachi X-650 microscope and a field-emission scanning electron microscope (JEOL-6300F, 15 kV). The transmission electron microscope (TEM) images, selected-area electron diffraction (SAED) pattern and high-resolution transmission electron microscope (HRTEM) image were recorded on a JEOL-2010 microscope. The room-temperature photoluminenscence (PL) spectra were performed on a Jobin Yvon-Labram spectrometer with a He–Cd laser at 325 nm. The Raman spectra were investigated with a French Labrum-HR cofocal laser micro-Raman spectrometer using an argon-ion laser at 514.5 nm. Gas-sensing measurements were performed with a WS-30A system (Weisheng Instruments Co., Zhengzhou, China). The samples used for SEM, TEM and HRTEM characterization were dispersed in absolute ethanol and were slightly ultrasonicated before observation.

2.4. Gas sensor measurements

Gas sensors were fabricated by using thin films prepared from a powder suspension of the as-prepared products. The materials were dispersed in ethylene glycol and ultrasonicated into slurry before fabricating the sensors. No conductive binder was added. The slurry was coated on a ceramic tube on which a pair of Au electrodes were previously printed, and subsequent calcination at 450 °C for 2 h in air.

3. Results and discussion

3.1. Morphology and structure

The structures of the as-synthesized SnO_2 nanorods (a) and hollow spheres (b) were determined by XRD, as shown in Fig. 1. All the diffraction peaks can be readily indexed to the tetragonal phase of SnO_2 with calculated lattice

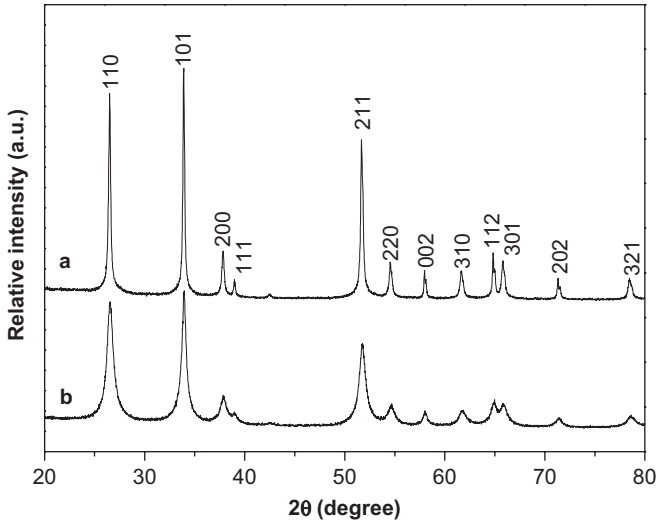

Fig. 1. XRD patterns of SnO_2 short nanorods (a) and hollow microspheres (b).

parameters of $a = 4.742$ Å and $c = 3.186$ Å, which are well in agreement with the reported values (JCPDS no. 77-0450). Both the samples exhibit high crystallinity. As can be seen from Fig. 1, the diffraction peaks of SnO_2 hollow spheres obviously broadened, which indicates the smaller particle size compared with nanorods. The relatively higher intensity of diffraction peaks of nanorods demonstrates the higher crystallinity. No impurity peaks are observed, indicating the high purity of the final products.

The Raman spectra shown in Fig. 2 further confirm the tetragonal rutile structure of the as-synthesized SnO_2 nanorods (a) and hollow spheres (b). There are four Raman shift peaks from our samples, and the Raman spectrum of SnO_2 nanorods is much similar to that of hollow spheres. Two fundamental Raman scattering peaks centered at wavenumbers of about 635 and 776 cm^{-1}, which usually appear in bulk single crystals or polycrystalline SnO_2 materials, can be observed from Fig. 2a. The peak at 635 cm^{-1} can be attributed to the A_{1g} symmetric Sn–O stretching mode in nanocrystalline SnO_2 and the peak at 776 cm^{-1} can be assigned to the B_{2g} vibrational mode. In addition to these classical modes, two Raman scattering peaks at about 354 and 576 cm^{-1} can be also observed, which is similar to the Raman spectra of SnO_2 nanorods [24] and nanocones [32] reported previously. Here, these additional Raman peaks may possibly be attributed to several specific factors. For example, some infrared-only active modes are now seen in the Raman spectrum owing to a break-down of selection rules or new modes named "surface modes" resulting from the vast increase of surface area [33,34].

The morphology and size of the initial SnO_2 nanorods (sample 1) and microspheres (sample 2) were investigated by TEM and FE-SEM. As can be seen from Fig. 3a and b, sample 1 consists of short nanorods with diameters of 10–15 nm and lengths ranging from 50 to 70 nm, which aggregate homocentrically together to form urchin-like nanostructures. We find many separated nanorods (Fig. 3b) have been broken off owing to the fact that the sample in absolute alcohol is dispersed to TEM detection by ultrasonic vibration. To further study the fine structures of the nanorods, HRTEM was analyzed. More detailed structural information for these nanorods was obtained from HRTEM (Fig. 3c and d) images and SAED pattern. The typical HRTEM image of an individual nanorod was shown in Fig. 3d. The spacing between the lattice planes along the length and the width of the nanorods are about 0.317 and 0.333 nm, which are well consistent with (0 0 1) and (1 1 0) planes of tetragonal SnO_2, respectively. This indicates that the nanorods grow along (0 0 1) direction. The inset of Fig. 3c shows the corresponding SAED pattern of the individual nanorod, indicating that the as-prepared nanorods are single crystalline in structure. Composition of SnO_2 nanorods has been characterized using EDS. The EDS spectrum (Fig. 3e) showed that components of the materials are Sn and O. The Cu and C signals are attributed to the grid used in the TEM measurement.

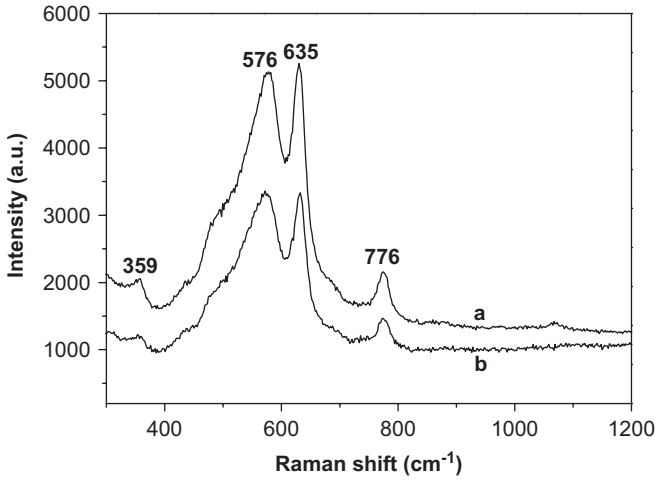

Fig. 2. Raman spectra of the SnO_2 nanorods (a) and hollow microspheres (b).

Sample 2 is composed of relatively uniform microspheres with diameters in the range of 2–3 μm, which can be confirmed from the FE-SEM images (Fig. 4a and b). A high-magnification FE-SEM image of one broken SnO_2 hollow microsphere was shown in Fig. 4c, from which we can see its hollow structure and clear grain boundary on the surface. It demonstrated that the as-obtained microspheres are constituted by aggregation of small SnO_2 particles, which is in good agreement with the XRD patterns. The TEM image (Fig. 4d) reveals the shell thickness of the hollow microspheres is about 60–140 nm and further confirms the hollow structures of SnO_2 microspheres.

Comparison experiments were conducted in order to study the growth process of the nanorods. Without adding HMT into the reaction system, the molar ratio between NaOH and $SnCl_2$ was found to be an important parameter that influences the SnO_2 particle morphology. For example, only irregular nanoparticles (see Fig. S1a) were obtained with a lower ratio of 4:1. When the ratio is increased to 6:1, urchin-like nanostructures assembled by short nanorods were obtained. When the ratio is as high as 9:1, conglomerations (Fig. 5a) assembled by some tetragonal square-based pyramid-shaped nanorods were fabricated. Upon further increasing the ratio to 12:1, no product but a clear solution was obtained. In this course, $Sn(OH)_6^{2-}$ ions formed at first after H_2O_2 and NaOH were added into $SnCl_2$ aqueous solutions (reaction (1)). Subsequently, $Sn(OH)_6^{2-}$ ions decomposed under hydrothermal conditions (reaction (2)). We supposed that the hydroxide ion plays a double role in the process. The basic medium is propitious to reaction (1), but too high basic concentration may be unfavorable for the reaction (2), thus, we obtained no products finally at a high molar ratio of NaOH to $SnCl_2$:

$$Sn^{2+} + H_2O_2 + 4OH^- \rightarrow Sn(OH)_6{}^{2-}. \quad (1)$$

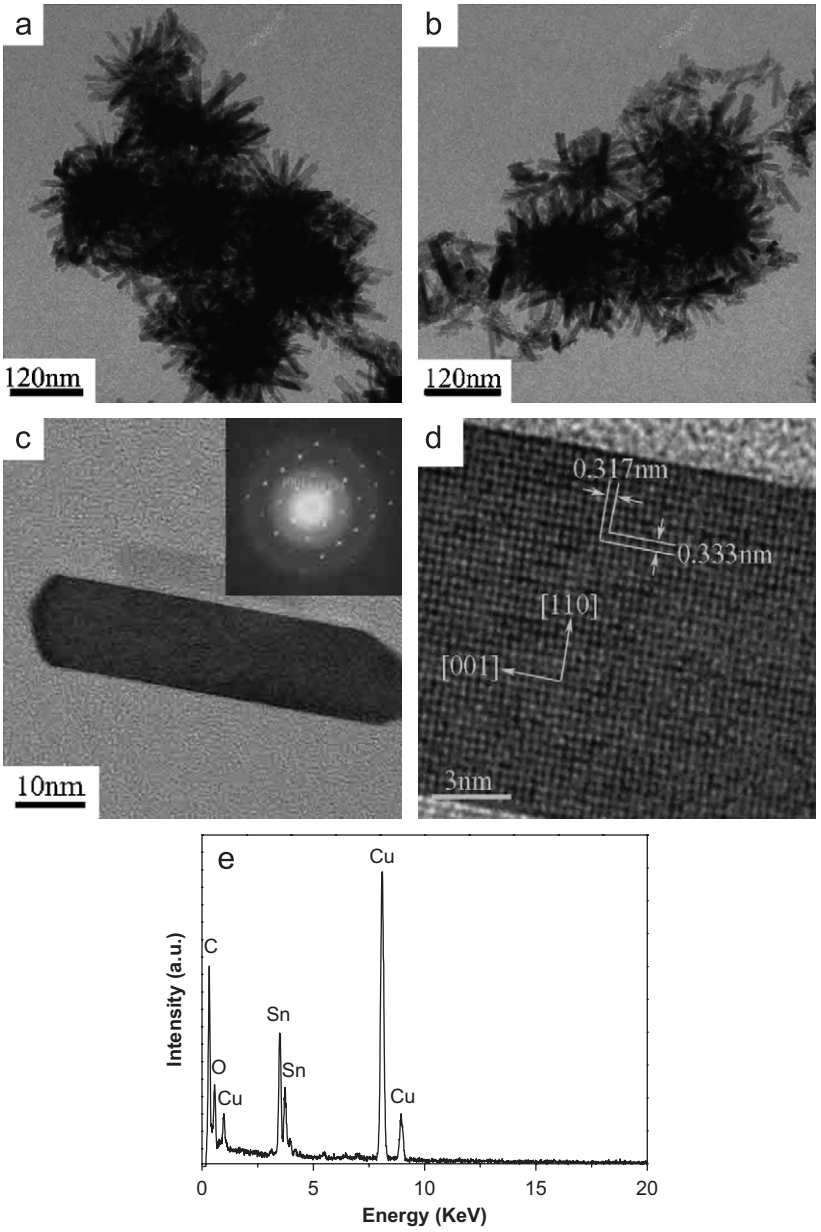

Fig. 3. (a and b) TEM images of SnO_2 nanorods. (c and d) HRTEM images of a single SnO_2 nanorod. The upper right inset in (c) is a SAED pattern from the individual nanorod. (e) A typical EDS spectrum of SnO_2 nanorods separated on a TEM grid.

$$Sn(OH)_6^{2-} \rightarrow SnO_2 + 2H_2O + 2OH^- . \quad (2)$$

In addition, the hydrothermal temperature is also an important factor affecting the growth of SnO_2. If the reaction was carried out at a low temperature of 140 °C, only irregular nanoparticles were obtained. Microspheres (Fig. 5b) with diameters in the range of 1–4 μm were formed when the temperature was kept at 160 °C. However, when increasing the hydrothermal temperature to 180 °C, short nanorods with lengths of 5–10 nm and diameters of 10–30 nm were prepared, coexisting with nanoparticles (see Fig. S1b). When the hydrothermal temperature increased to 200 °C, urchin-like nanostructures composed of uniform short nanorods with diameters of 10–15 nm and lengths of 50–70 nm were obtained.

In order to reveal the possible mechanism in the formation of SnO_2 nanorods, a lot of detailed time-dependent experiments were carried out. When the reaction lasted for 5 h, some aggregated particles were received; when the reaction time was prolonged to 15 h, urchin-like shapes composed of some radially short nanorods (see Fig. S2) appeared, and some irregular nanoparticles can still be observed. When the reaction time was extended to 30 h, the products were urchin-like shapes self-assembled by nanorods with diameters of 10–15 nm and lengths of 50–70 nm. On the basis of the above experiments, at the initial stage of hydrothermal reaction, the SnO_2

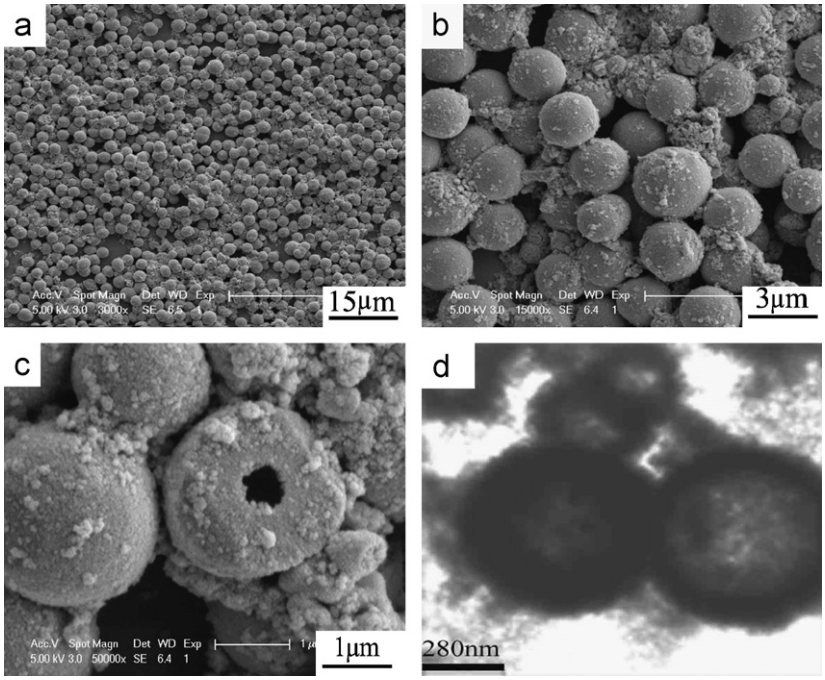

Fig. 4. Low-magnification FE-SEM image (a) and high-magnification FE-SEM image (b) of SnO_2 microspheres and high-magnification FE-SEM image (c) of a broken SnO_2 hollow microsphere and the TEM image (d) of SnO_2 hollow microspheres, respectively.

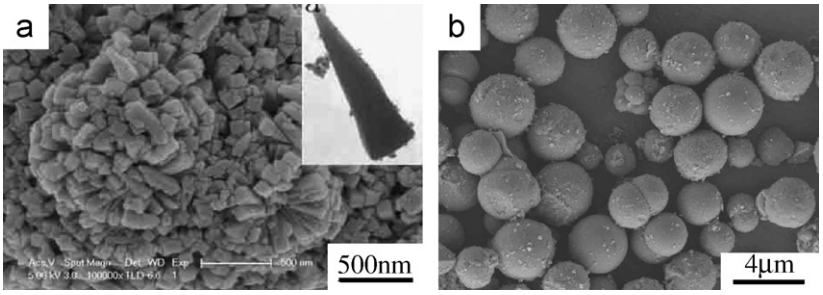

Fig. 5. TEM (inset in (a)) and FE-SEM images of SnO_2 in different reaction conditions: (a) M_{NaOH}:M_{SnCl_2} = 9:1 at 200 °C for 30 h and (b) M_{NaOH}:M_{SnCl_2} = 6:1 at 160 °C for 30 h, respectively.

precipitated out as nanoparticles with small size, and then these particles grew into radial nanorods through aggregation mechanism [23] and Ostwald ripening [35] process. Of course, a detailed understanding of SnO_2 nanorods formation mechanism needs further investigation.

The difference between the formation of SnO_2 nanorods and hollow microspheres is the involvement of $(CH_2)_6N_4$, which is a nontoxic, water-soluble, nonionic tetradentate cyclic tertiary amine [36] and has been applied to the synthesis of ZnO nanomaterials [37,38]. Here, similar to the preparation of CuO hollow microspheres [39], $(CH_2)_6N_4$ played a crucial part in the formation of SnO_2 hollow microspheres. Under hydrothermal conditions, $Sn(OH)_6^{2-}$ decomposed into small SnO_2 nanoparticles, and $(CH_2)_6N_4$ hydrolyzed [40] to provide NH_3 gas as the soft template to fabricate hollow microspheres. The reaction at basic conditions can be shown as follows:

$$Sn^{2+} + H_2O_2 + 4OH^- \rightarrow Sn(OH)_6{}^{2-},$$

$$Sn(OH)_6{}^{2-} \rightarrow SnO_2 + 2H_2O + 2OH^-,$$

$$(CH_2)_6N_4 + 6H_2O \rightarrow 6HCHO + 4NH_3.$$

At the initial stage, small SnO_2 nanoparticles were generated, while microbubbles of NH_3 produced in the reaction provide the aggregation centers for these nanocrystals. In order to lower its interfacial free energies at the circinal edges between NH_3 and water, these SnO_2 nanoparticles have a tendency to aggregate around the gas–liquid interface between NH_3 and water to form a hollow microsphere. Scheme procedure used for the synthesis of SnO_2 hollow microspheres is shown in Fig. 6.

3.2. Photoluminescence and gas sensor property

Fig. 7 shows the room-temperature PL spectra of the as-prepared SnO_2 nanorods (a) and hollow microspheres (b), which were recorded with an excited wavelength of 325 nm.

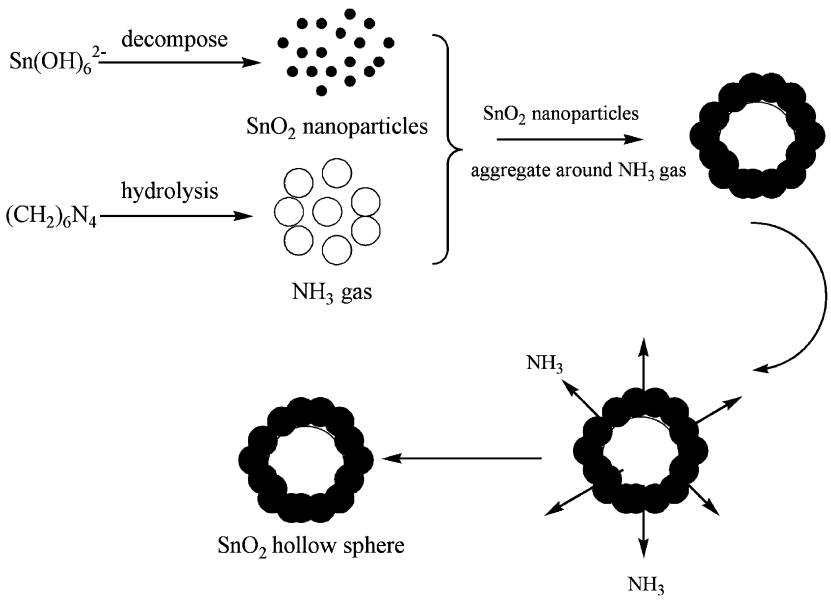

Fig. 6. Schematic illustration describing the formation of a hollow SnO_2 microsphere.

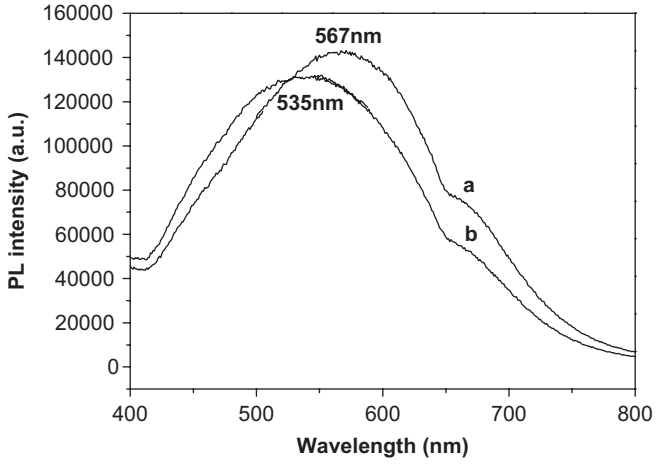

Fig. 7. The PL spectra of SnO_2 nanorods (a) and hollow microspheres (b) at room temperature with excited wavelength centered at 325 nm.

A broad green emission band centered at 567 nm is observed in the spectrum of the SnO_2 nanorods and that centered at 535 nm is also observed in the spectrum of hollow microspheres. The above observed peak positions are different from those observed in SnO_2 ribbons [9] and beak-like SnO_2 nanorods [12] which centered at about 605 nm. Compared with standard SnO_2 powder (at 575 nm) [9], the peak position of SnO_2 hollow spheres has a blue-shift of approximately 40 nm, while the peak position of SnO_2 nanorods shows no obvious change. A similar green emission centered at about 546 nm has been reported in the case of SnO_2 hollow microspheres [26]. It is well known that the morphology and size of materials have a great influence on their properties [41,42]. We believe that the strong PL peaks might be related to crystalline defects produced during the growth course, and the blue-shift might be attributed to the size-confinement effect of SnO_2 materials.

As an n-type semiconductor, SnO_2 has been widely investigated in applications in many surface-related properties, such as gas sensitivities. As described in Section 2, the samples used for gas sensitivity experiments experienced 2 h calcination at 450 °C before the measurements. It is important to elucidate the influence of the calcination made on the morphology of the SnO_2 nanocrystals. TEM and SEM observations indicated that the structures of the materials were not destroyed after the pretreatment process (see Fig. S5).

The gas sensitivity, in general, was defined as $S = R_{air}/R_{gas}$, where R_{air} and R_{gas} were the resistances of a gas sensor in the air and in a detected gas, respectively. Fig. 8a shows the changes in sensitivity of the as-prepared SnO_2 materials when a thin-film sensor was exposed to several gases with various concentrations. We can see that SnO_2 hollow microspheres have relatively high sensitivity to ethanol and methanol while the SnO_2 urchin-like structures have relatively weak sensitivity to methanol. SnO_2 hollow microspheres have higher sensitivity to methanol compared with SnO_2 nanorods and also have higher sensitivity to ethanol than to methanol. It is obvious that SnO_2 hollow microspheres have better gas sensor performance than nanorods. And the sensitivity gradually increases with an increasing concentration of the detected gases. Fig. 8b presents the variation in sensitivity of SnO_2 hollow spheres with ethanol concentration ranging from 40 to 80 ppm at room temperature. The results show that SnO_2 hollow spheres still have high sensitivity even with lower ethanol concentration, which is comparable to SnO_2 nanospheres [28] reported formerly. On increasing the concentration of the detected gas, the sensitivity in the low concentration shows approximate linearity. The SnO_2 hollow spheres also

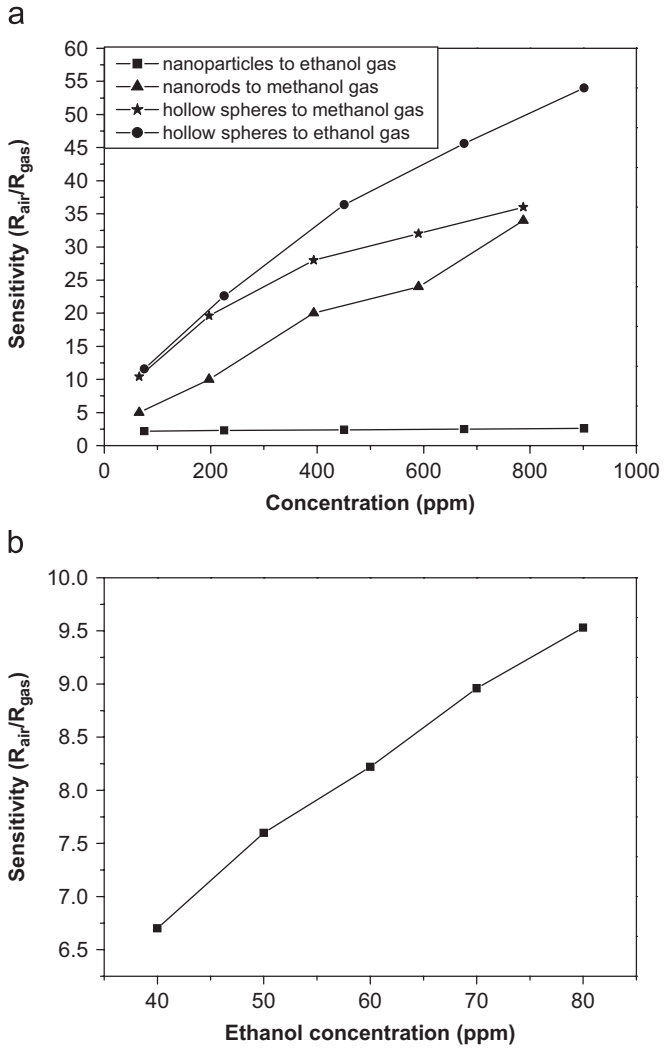

Fig. 8. Typical variations in sensitivity at room temperature with the change in concentration of the detected gases (a) and variation in sensitivity of SnO_2 hollow spheres with lower ethanol concentration (40–80 ppm) at room temperature (b).

have sensitivity to formaldehyde (see Fig. S4). SnO_2 nanorods show very weak sensitivity to ethanol, so typical variations in sensitivity with the change in concentration of ethanol is not shown here. The stability of those gas sensors was detected by repeating the test several times. After lots of cycling tests, no appreciable variations were detected. In order to evaluate the sensitivity of the as-synthesized SnO_2 materials, SnO_2 nanoparticles with the average size of 3.7 nm fabricated according to Ref. [43] were adopted as the reference with which to compare the room-temperature sensitivity to ethanol under the same experimental conditions. We can find that the sensitivity of the SnO_2 hollow spheres versus ethanol concentration was much greater than that of the SnO_2 nanoparticles. It demonstrated that the SnO_2 hollow microspheres and nanorods may be of great potential value in fabricating gas sensors.

According to previous reports [44,45], the sensitivity to the target gas strongly depends on the ease of diffusion of gas molecules inside the sensor. Thus, the structure and morphology of the particles can be correlated with the sensor performance. Higher surface area could enhance the interaction between SnO_2 surface and gas molecules to be detected, and the hollow structure would facilitate fast and full gas access to SnO_2 nanocrystals. The as-prepared SnO_2 materials are hence expected to offer advantages in fabricating gas sensors. The hollow structure is obviously far more favorable for the diffusion of gas molecules than that of a sensor constructed from the urchin-like structures. Therefore, the SnO_2 hollow microspheres provide better gas sensitivity compared with SnO_2 urchin-like structures.

4. Conclusions

In summary, SnO_2 urchin-like structures composed of short nanorods have been successfully synthesized via a simple H_2O_2-assisted hydrothermal method in the absence of any surfactant. With the addition of methenamine (HMT), SnO_2 hollow microspheres with diameter of 2–3 μm and shell thickness of 60–140 nm were obtained. The gas sensitivity experiments showed that the SnO_2 hollow microspheres offered better sensitivity than SnO_2 nanorods. It demonstrated that the SnO_2 hollow microspheres and nanorods may be of great potential value in fabricating gas sensors.

Acknowledgments

This work was supported by the National Natural Science Foundation of China (No. 20431020) and the 973 Project of China (No. 2005CB623601). The authors would also like to thank Weihong Xu, Zheng Guo and Professor Jinhuai Liu for their assistance in measurements.

Appendix A. Supporting information available

Typical TEM images and XRD patterns of the products prepared in different reaction conditions; TEM images and XRD patterns of the products prepared at different reaction time; typical variations in sensitivity at room temperature with the change in concentration of formaldehyde; TEM and SEM images of the products after calcination.

Appendix B. Supplementary data

Supplementary data associated with this article can be found in the online version at doi:10.1016/j.jssc.2007.11.010.

References

[1] A. Kolmakov, Y. Zhang, G. Cheng, M. Moskovits, Adv. Mater. 15 (2003) 997.
[2] M. Law, H. Kind, F. Kim, B. Messer, P.D. Yang, Angew. Chem. Int. Ed. 41 (2002) 2405.

[3] C. Goebbert, M.A. Aegerter, D. Burgard, R. Nass, H. Schmidt, J. Mater. Chem. 9 (1999) 253.
[4] J.S. Swinnea, J. Mater. Res. 8 (1993) 3131.
[5] P.G. Harrison, M.J. Willet, Nature 332 (1988) 337.
[6] S. Ferrere, A. Zaban, B.A. Gregg, J. Phys. Chem. B 101 (1997) 4490.
[7] Z.R. Dai, J.L. Gole, J.D. Stout, Z.L. Wang, J. Phys. Chem. B 106 (2002) 1274.
[8] S.H. Luo, J.Y. Fan, W.L. Liu, M. Zhang, Z.T. Song, C.L. Lin, X.L. Wu, P.K. Chu, Nanotechnology 17 (2006) 1695.
[9] J. Hu, Y. Bando, Q. Liu, D. Golberg, Adv. Funct. Mater. 13 (2003) 493.
[10] J.Q. Hu, X.L. Ma, N.G. Shang, Z.Y. Xie, N.B. Wong, C.S. Lee, S.T. Lee, J. Phys. Chem. B 106 (2002) 3823.
[11] J.Q. Sun, J.S. Wang, X.C. Wu, G.S. Zhang, J.Y. Wei, S.Q. Zhang, H. Li, D.R. Chen, Cryst. Growth & Des. 6 (2006) 1584.
[12] J.H. He, T.H. Wu, C.L. Hsin, K.M. Li, L.J. Chen, Y.L. Chueh, L.J. Chou, Z.L. Wang, Small 2 (2006) 116.
[13] R.S. Yang, Z.L. Wang, J. Am. Chem. Soc. 128 (2006) 1466.
[14] Y. Wang, J.Y. Lee, C.H. Zeng, Chem. Mater. 17 (2005) 3899.
[15] S.J. Han, B.C. Jang, T. Kim, S.M. Oh, T.H. Hyeon, Adv. Funct. Mater. 15 (2005) 1845.
[16] Q.R. Zhao, Z.G. Zhang, T. Dong, Y. Xie, J. Phys. Chem. B 110 (2006) 15152.
[17] Z.W. Pan, Z.R. Dai, Z.L. Wang, Science 291 (2001) 1947.
[18] Z.R. Dai, Z.W. Pan, Z.L. Wang, Solid State Commun. 118 (2001) 351.
[19] S. Mathur, S. Barth, H. Shen, J.C. Pyun, U. Werner, Small 1 (2005) 713.
[20] Q.R. Zhao, Z.G. Zhang, T. Dong, Y. Xie, J. Nanopart. Res. 8 (2006) 1065.
[21] J.S. Wang, J.Q. Sun, G.S. Zhang, X.C. Wu, Y. Bao, H. Li, D.R. Chen, Mater. Lett. 60 (2006) 2600.
[22] Y.L. Wang, X.C. Jiang, Y.N. Xia, J. Am. Chem. Soc. 125 (2003) 16176.
[23] D.F. Zhang, L.D. Sun, J.L. Yin, C.H. Yan, Adv. Mater. 15 (2003) 1022.
[24] B. Cheng, J.M. Russell, W.S. Shi, L. Zhang, E.T. Samulski, J. Am. Chem. Soc. 126 (2004) 5972.
[25] L. Vayssieres, M. Graetzel, Angew. Chem. Int. Ed. 43 (2004) 3666.
[26] W.P. Shao, Z.H. Wang, Y.G. Zhang, J.H. Cui, W.C. Yu, Y.T. Qian, Chem. Lett. 34 (2005) 556.
[27] F.L. Du, Z.Y. Guo, G.C. Li, Mater. Lett. 59 (2005) 2563.
[28] Q.R. Zhao, Y. Gao, X. Bai, C.Z. Wu, Y. Xie, Eur. J. Inorg. Chem. (2006) 1643.
[29] X.W. Lou, Y. Wang, C.L. Yuan, J.Y. Lee, L.A. Archer, Adv. Mater. 18 (2006) 2325.
[30] Q.H. Cao, Y.Q. Gao, X.Y. Chen, L. Mu, W.C. Yu, Y.T. Qian, Chem. Lett. 35 (2006) 178.
[31] C.H. Ye, X.S. Fang, Y.H. Wang, T. Xie, A.W. Zhao, L.D. Zhang, Chem. Lett. 33 (2004) 54.
[32] G. Cheng, J.M. Wang, X.W. Liu, K.X. Huang, J. Phys. Chem. B 110 (2006) 16208.
[33] A. Dieguez, A. Romano-Rodriguez, A. Vila, J.R. Morante, J. Appl. Phys. 90 (2001) 1550.
[34] L. Abello, B. Bochu, A. Gaskov, S. Koudryavtseva, G. Lucazeau, M. Roumyantseva, J. Solid State Chem. 135 (1998) 78.
[35] Z.P. Liu, S. Li, Y. Yang, S. Peng, Z.K. Hu, Y.T. Qian, Adv. Mater. 15 (2003) 1946.
[36] L. Vayssieres, K. Keis, A. Hagfeldt, S.E. Lindquist, Chem. Mater. 13 (2001) 4395.
[37] Y. Shu, S. Tsugio, J. Mater. Chem. 15 (2005) 4584.
[38] H.H. Wang, C.S. Xie, D.W. Zeng, Chem. Lett. 34 (2005) 260.
[39] Y.G. Zhang, S.T. Wang, Y.T. Qian, Z.D. Zhang, Solid State Sci. 8 (2006) 462.
[40] B. Deng, A.W. Xu, G.Y. Chen, R.Q. Song, L.P. Chen, J. Phys. Chem. B 110 (2006) 11711.
[41] A.P. Alivisatos, Science 271 (1996) 933.
[42] A.M. Morales, C.M. Lieber, Science 279 (1998) 208.
[43] S.P. Gong, C. Xu, H. Liu, Rare Metal Mater. Eng. 35 (2006) 583.
[44] G. Sakai, N. Matsunaga, K. Shimanoe, N. Yamazoe, Sens. Actuators B 80 (2001) 125.
[45] N. Matsunaga, G. Sakai, K. Shimanoe, N. Yamazoe, Sens. Actuators B 83 (2002) 216.